

EMF Exposure Mitigation via MAC Scheduling

Silvio Mandelli, Lorenzo Maggi, Bill Zheng, Azra Zejnilagic, Christophe Grangeat
Nokia. E-mail: silvio.mandelli@nokia-bell-labs.com

Abstract—International standards bodies define Electromagnetic field (EMF) emission requirements that can be translated into control of the base station *actual* Effective Isotropic Radiated Power (EIRP), i.e., averaged over a sliding time window. In this work we show how to comply with such requirements by designing a water-filling power allocation method operating at the MAC scheduler level. Our method ensures throughput fairness across users while constraining the EIRP to a value that is produced by an outer-loop procedure which is not the focus of our paper. The low computational complexity of our technique is appealing given the tight computational requirements of the MAC scheduler.

Our proposal is evaluated against the prior art approaches through massive-MIMO system level simulations that include realistic modeling of physical and MAC level cellular procedures. We conclude that our proposal effectively mitigates EMF exposure with considerably less impact on network performance, making it a standout candidate for 5G and future 6G MAC scheduler implementations.

Index Terms—EMF exposure, EIRP control, 5G, 6G, MAC Scheduling, Massive-MIMO.

I. INTRODUCTION

Fifth generation (5G) cellular network deployments are characterized by the use of massive Multiple Inputs Multiple Outputs (MIMO) techniques which ensure high user throughput but also increases Radio Frequency (RF) electromagnetic field (EMF) exposure. This trend is expected to continue in sixth generation (6G) extreme-MIMO deployments, where hundreds or even thousands antenna elements, with higher beam gains than in 5G, are envisioned [1].

When assessing a base station compliance with RF EMF exposure limits [2], the actual maximum approach described in [3] takes into account the *actual* Effective Isotropic Radiated Power (EIRP), i.e., averaged over a time window of 6 to 30 minutes. This window plays a significant role in the assessment of EMF exposure from base stations, due to the variability of their EMF emissions in time and in space. Channel modelling studies showed that the actual EIRP threshold is typically a factor 0.25 below the configured maximum EIRP [4], but lower values can be foreseen with advanced beamforming algorithms [5].

Imposing real-time constraints on EIRP in cellular networks requires modifying the Medium Access Control (MAC) scheduler operations. This is no easy task, due to the scheduler complexity and the tight computation latency constraint. Existing approaches [6], [7] propose power control procedures limiting the usable bandwidth; [8] optimizes precoding for MIMO systems under the assumption of full channel knowledge. However, this assumption is unfeasible in reality as it would require heavy inter-working between physical and

MAC layer. Finally, imposing EIRP constraints affects network performance when reaching the actual EIRP threshold [4], highlighting the importance of designing algorithms that minimize the performance degradation while being implementable in MAC layer real-time procedures.

Our contribution. We consider the framework illustrated in Fig. 1, where an “outer-loop” mechanism operates on a slow time scale, monitoring the actual EIRP over a sliding window of a few minutes, as prescribed in [3]. Such mechanism sets the EIRP budget for the next “period” which encompasses the next few hundred of slots. The design of the outer-loop mechanism is not the focus of this paper and can be found, e.g., in [9]. In this paper we focus on the “inner-loop” aspect depicted in Fig. 1, which enforces the EIRP budget in real-time via MAC scheduling operations. Initially, the subset of User Equipments (UEs) eligible for transmission in the current slot is selected as described, e.g., in [10]. Then, the EIRP is controlled by allocating Physical Resource Blocks (PRBs), power and Modulation and Coding Scheme (MCS) *fairly* across UEs. Our proposal comprises two subroutines: the first spreads the EIRP budget across slots within the same period, to accommodate traffic bursts while avoiding budget depletion before the period ends. The second subroutine performs a *fair* allocation across the UEs while fulfilling the constraint on the per-slot EIRP budget.

Prior art [6], [7] proposed constraining resources solely in the frequency, i.e., PRB, domain to limit EIRP. Instead, we propose dynamically adjusting the user MCS and power to maximize the global UE throughput fairness while adhering to an EIRP constraint. The concept of reducing MCS and power while spreading the transmission across more radio time and frequency resources was already introduced in [11], [12]. Yet, constraints on EIRP were not considered since the primary focus was mitigating interference in non-full buffer scenarios.

Our intuition suggests that, to control EIRP, reducing power similarly to the approach in [11], [12] should be preferred over reducing bandwidth. This reasoning stems directly from the classic Shannon formula: reducing bandwidth leads to a linear decrease in both rate and EIRP, while decreasing power results in a *logarithmic* reduction in rate. These effects tend to coincide in the low SINR regime. Therefore, we expect power-based EIRP control solutions to drastically outperform bandwidth based approaches, if properly implemented. As a side-product, overall network interference will be reduced, as demonstrated in [11], [12].

We evaluate our proposal in a highly realistic 3rd Generation Partnership Project (3GPP) calibrated simulation setup, with a full physical and MAC implementation of a massive-MIMO

cellular scenario. The results enable us to draw conclusions regarding the potential architecture and algorithms for deployment in a MAC scheduler of a g-Node B (gNB) in cellular networks to control EIRP with minimal impact on system performance.

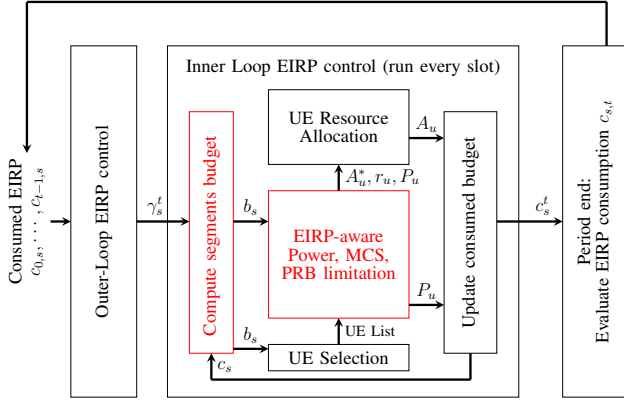


Fig. 1: Block diagram of EIRP control operations considered in this work. Slot index k has been omitted in inner-loop operations for readability. The main focus of our work concerns the red blocks, while the other parts are either legacy MAC scheduling operations in the inner-loop, or outer-loop operations discussed in [9].

II. EMF EXPOSURE MODEL

We address the downlink (DL) scheduling problem of allocating PRBs and power to users while mitigating the human exposure to EMF according to [3]. We first introduce some notation. We let $A_{u,k}$ and $P_{u,k}$ be the number of allocated PRBs and the transmit power per PRB for user u in slot k , respectively. We denote by $\beta_{u,k}$ the beam serving user u in slot k and we call $G_{u,k}(\phi, \theta)$ the antenna gain in azimuth/elevation direction (ϕ, θ) when beam $\beta_{u,k}$ is used. The set of *active* UEs, i.e., the UEs with DL data in the buffer, is \mathcal{U}_k . The EIRP emitted by a radiating antenna array in the azimuth/elevation direction (ϕ, θ) in slot k writes:

$$\text{EIRP}_k(\phi, \theta) := \sum_{u \in \mathcal{U}_k} A_{u,k} P_{u,k} G_{u,k}(\phi, \theta). \quad (1)$$

The power density measured at distance R from the antenna in the direction (ϕ, θ) is proportional to the EIRP, and equals $\frac{\text{EIRP}(\phi, \theta)}{4\pi R^2}$ in free space conditions. When implementing the so-called “actual maximum approach” described in [3], the *actual* EIRP, i.e., time averaged over a sliding window, of the base station shall not exceed a configured actual EIRP threshold \bar{C} . Depending on the environment, different thresholds may need to be configured in different directions. To account for this, we partition the set of all azimuth/elevation angles, defined with respect to the radiating antenna, into a set of *segments* \mathcal{S} , and assign a specific actual EIRP threshold \bar{C}_s to each segment $s \in \mathcal{S}$. We then define the EIRP *consumption* $c_{k,s}$ as the maximum EIRP in segment s :

$$c_{k,s} := \max_{(\phi, \theta) \in \mathcal{S}} \text{EIRP}_k(\phi, \theta). \quad (2)$$

We call *period* t a set of $K \geq 1$ consecutive slots starting from k_0^t , and we define $c_s^t := \sum_{k=k_0^t}^{k_0^t+K-1} c_{k,s}$ the sum of EIRP consumption over period t . To comply with [3], we impose that the *actual* EIRP, i.e., the average EIRP consumption over every sliding window of W consecutive periods, does not exceed \bar{C}_s , for each segment s :

$$\frac{1}{W} \sum_{i=0}^{W-1} c_s^{t-i} \leq \bar{C}_s, \quad \forall t. \quad (3)$$

III. POWER CONTROL FOR EMF EXPOSURE MITIGATION

As illustrated in Fig. 1, an outer-loop algorithm computes the limit γ_s^t on the EIRP consumption in period t , such that

$$0 \leq c_s^t \leq \gamma_s^t, \quad \forall t, s \in \mathcal{S}. \quad (4)$$

The design of the outer-loop algorithm is not the focus of this paper and is discussed, e.g., in [9]. Then, we consider γ_s^t as a predefined input for each s, t . In this paper we study how to enforce the EIRP cap (4) on a per-slot and on a per-user basis via a so-called *inner-loop* control mechanism within DL MAC scheduler operations depicted in Fig. 1.

Without loss of generality we consider $k_0^t = 1$. We then split our problem into two sub-problems that we solve separately.

- 1) **Per-slot EIRP constraint.** For each segment s and in each period t , it must hold that $\sum_{k=1}^K c_{k,s} \leq \gamma_s^t$. We smooth out the EIRP consumption over time by computing an upper limit - or *slot budget* - $b_{k,s}$ for $c_{k,s}$, for each slot k and segment s .
- 2) **Power allocation.** At slot k , we allocate power fairly across UEs by ensuring $c_{k,s} \leq b_{k,s}$.

For simplicity of notation, we hereafter drop the dependence of variables on period t .

A. Per-slot EIRP constraint design

Let us fix the segment s . At the beginning of each slot $k = 1, \dots, K$, given the past consumption $c_{1,s}, \dots, c_{k-1,s}$, we must cap the EIRP consumption for the upcoming slot to a value $b_{k,s}$. We propose to inject a portion $(1 - \epsilon_s)$ of the period’s budget γ_s at slot $k = 0$ and spread the remainder by injecting $\epsilon_s \gamma_s / K$ at each slot, with $0 \leq \epsilon_s \leq 1$. Therefore, the available slot budget at slot k is

$$b_{k,s} = \max \left(\left(1 - \epsilon_s \frac{K-k}{K} \right) \gamma_s - \sum_{i=1}^{k-1} c_{i,s}, 0 \right). \quad (5)$$

The difficulty in designing the portion ϵ_s resides in the fact that future user requests are unknown. On the one hand, we want to avoid to greedily deplete the budget early on in the period with ϵ_s close to zero, which would lead to empty slots later on. On the other hand, we want to refrain from introducing unnecessarily delay by curbing consumption in an overly conservative manner with ϵ_s close to one.

Similarly, we would like to avoid the possible excessively low slot budget as computed in (5). Therefore, the slot budget can be lower bounded by $\rho_s^* c_s^*$, where c_s^* is the maximum EIRP that can be radiated in the segment s in one slot on all

available PRBs and full power and maximum beam gain, and $0 < \rho_s^* c_s^* < \gamma_s/K$.

Optionally, we propose to start curbing EIRP once the slot budget is below a certain guard threshold b_s^* , controlling EIRP emission before the slot budget gets too low. Therefore, we also study the following slot budget refinement

$$b'_{k,s} = c_s^* \exp(\ln(\rho_s^*) \max(1 - b_{k,s}/b_s^*, 0)). \quad (6)$$

B. Power Limiting (PL) techniques

We now show how to enforce the EIRP constraint $b_{k,s}$ on segment s by allocating power to active UEs in a fair manner. We assume that $A_{u,k}$ PRBs have been pre-allocated to each active UE $u \in \mathcal{U}_k$ as a function of—amongst others—the amount of bits present in the buffer for each UE, the selected MCS and the corresponding rate m_u, r_u , respectively. In our preferred implementation, this is performed via the method described in [12], which downgrades the UEs' MCS and reduces the transmit power accordingly, hence increasing the required PRB allocation, but without exceeding the PRBs available in the current slot. As a result, the transmit power and resulting interference in neighbouring cells are reduced.

Two simplifying approximations. Since power allocation must be decided at every slot, computational complexity is a bottleneck. To simplify the problem we first approximate that each beam β has positive gain only in one segment $s(\beta)$, i.e., the one containing its main lobe. We call $\mathcal{U}_{k,s} \subset \mathcal{U}_k$ the set of active users served by a beam whose main lobe is in segment s , i.e., $\mathcal{U}_{k,s} := \{u \in \mathcal{U}_k : s(\beta_{u,k}) = s\}$. Then, the estimated EIRP consumption $\hat{c}_{k,s}$ depends only on users $\mathcal{U}_{k,s}$:

$$\hat{c}_{k,s} = \max_{(\phi, \theta) \in s} \sum_{u \in \mathcal{U}_{k,s}} A_{u,k} P_{u,k} G_{u,k}(\phi, \theta) \quad (7)$$

and the power allocation $P_{u,k}$ for a user in $\mathcal{U}_{k,s}$ does not impact the EIRP consumption over a different segment $s' \neq s$. In this case, we can optimize the user power allocation for the current slot k independently for each segment.

Next, computing $\hat{c}_{k,s}$ as in (7) requires the solution of an optimization problem. To circumvent it and simplify computations, we pre-compute the maximum gain for each beam:

$$\hat{G}_{u,k} := \max_{(\phi, \theta) \in s} G_{u,k}(\phi, \theta) \quad (8)$$

and we bound $\hat{c}_{k,s}$ via a simple-to-compute expression, that must then be lower or equal than the slot budget:

$$\hat{c}_{k,s} \leq \sum_{u \in \mathcal{U}_{k,s}} A_{u,k} P_{u,k} \hat{G}_{u,k} \leq b_{k,s}. \quad (9)$$

Note that equality in (9) holds only if the gain is maximal in the same direction for all beams serving users in $\mathcal{U}_{k,s}$. Moreover, the available budget in the current slot is computed in (5)-(6) with respect to the *actual*, i.e., not approximate, past EIRP consumption values $c_{.,s}$ that are measured in hindsight.

Optimization problem. We now formulate the problem of power allocation across UEs. For notation simplicity we drop the variable dependence on s, k , with the understanding that the same procedure is used at each slot k and segment s .

Let $r_u(P_u)$ be the function mapping the power allocated to user u to its transmission rate per PRB. In practice, r_u is a staircase increasing function that can be well approximated as a continuous *concave* function, e.g., $r_u(P_u) = w \log(1 + P_u/N_u)$ where N_u is the noise plus interference PSD and w is an appropriate constant for the data channel codes used.

We allocate power across UEs by maximizing a fairness function of the UE throughput under the EIRP constraint. To this aim, we introduce the fairness function [13]:

$$f_\alpha(x) := \begin{cases} \frac{x^{1-\alpha}}{1-\alpha} & \text{if } \alpha \geq 0, \alpha \neq 1 \\ \log(x) & \text{if } \alpha = 1 \end{cases} \quad (10)$$

and we formulate our power allocation problem for each segment $s \in \mathcal{S}$ and slot k as follows:

$$\max_{\{P_u\}} \sum_{u \in \mathcal{U}} f_\alpha(A_u r_u(P_u)) \quad (11a)$$

$$\text{s.t.} \quad \sum_{u \in \mathcal{U}} A_u P_u \hat{G}_u \leq b \quad (11b)$$

$$\underline{P}_u \leq P_u \leq \bar{P}_u, \quad \forall u \in \mathcal{U}. \quad (11c)$$

where in (11b) we used the consumption upper bound (9).

Note that, if $\alpha = 1$, then the objective function (11a) maximizes the proportional fairness of the throughput across UEs; as α grows, it tends to max-min fairness [13]. The lower power value $\underline{P}_{u,k}$ can be chosen such that reception is possible with the most robust modulation and coding scheme available.

Water-filling solution. Problem (11) is convex, with separable objective function and subject to linear constraints. Hence, if the feasibility region contains an interior point (known as Slater condition [14]), which holds if \underline{P}_u 's are sufficiently low, then Karush-Kuhn-Tucker (KKT) conditions are necessary and sufficient conditions for optimality [14]. In our case, KKT conditions lead to the following water-filling type solution.

Define the class of power allocations $\{P_u^*(\nu)\}_u$, depending on the value of a parameter (read, Lagrangian multiplier) ν :

$$P_u^*(\nu) = \begin{cases} \bar{P}_u, & \text{if } (A_u \hat{G}_u)^{-1} \frac{d}{dP_u} f_\alpha(A_u r_u(\bar{P}_u)) > \nu \\ \underline{P}_u, & \text{if } (A_u \hat{G}_u)^{-1} \frac{d}{dP_u} f_\alpha(A_u r_u(\underline{P}_u)) < \nu \\ P^* : (A_u \hat{G}_u)^{-1} \frac{d}{dP_u} f_\alpha(A_u r_u(P^*)) = \nu, & \text{else} \end{cases} \quad (12)$$

Then, the solution to the problem (11) is $P_u^* = P_u^*(\nu^*)$ for all UEs u , where ν^* is the ‘‘water level’’ such that:

$$\nu^* = \max \left\{ \nu : \sum_u A_u \hat{G}_u P_u^*(\nu) \leq b \right\}. \quad (13)$$

Note that computing ν^* in (13) requires one to find the root of the function $\nu \rightarrow \sum_u A_u \hat{G}_u P_u^*(\nu) - b$, which can be solved numerically via, e.g., the classic bisection method.

IV. SIMULATIONS

Our simulation experiments are performed in a DL system-level simulator implementing a 3GPP calibrated Urban Macro (UMa) [15] channel model, abstracting the physical-layer effects through a link to system-level interface computing

equivalent Signal to Interference plus Noise Ratio (SINR) at transmission time, given the cell/user topology and the beamformed active transmissions in each cell. The simulation environment consists of a hexagonal deployment of seven three-sector sites at 500 m inter-site distance, corresponding to 21 cells with gNB installed at 25 m height and 12 degrees mechanical downtilt. The main simulation parameters can be found in Table I. The central frequency is at 3.5 GHz, with 273 PRBs at 30 kHz subcarrier spacing generating a 100 MHz carrier in Time Division Duplex (TDD) split, with an average ratio of 4 DL slots every uplink (UL) slot, with a total simulation time of 12 seconds. In our considered scenario the gNBs are equipped with a uniform rectangular array of 12×8 cross-polarized antennas with 5.2 dBi gain. The UEs have 2 cross-polarized omni-directional antenna elements. The antenna spacing is defined in multiple of the wavelength λ in Table I. The wideband Channel Quality Indicator (CQI) report is provided every 160 ms to the gNB, with measurements taken every 80 ms. DL Beamforming is based on Sounding Reference Signals transmitted by the UEs in UL, with beams selected among a codebook of Discrete Fourier Transform (DFT) beams [16] in the two-dimensional angular (ϕ, θ) plane. The UEs generate traffic according to the 3GPP File Transfer Protocol 2 (FTP2) traffic model [17], where each UE starts downloading a new packet of Q bits 50 ms after its previous packet was successfully downloaded. The MAC scheduler architecture is depicted in Fig. 1. At most 8 UEs per slot are selected according to proportional-fair metrics in the “UE selection” block, and after the possible actions due to actual EIRP control, finally the available PRBs are allocated to them with a round robin criterion with single-user MIMO allocations for up to 4 layers. In accordance to the proportional-fair criterion, we chose $\alpha = 1$ in (11).

General Environment	3GPP UMa [15], no buildings
Cells deployment	7×3 sector sites at 500 m distance
Traffic model	210 FTP2 [17], Reading time 50 ms
CQI feedback	Wideband reports every 160 ms
CQI/MCS Table	CQI/MCS Table 2, 256 QAM [18]
Link Performance	3GPP data channel codes [18]
Central Frequency	3.5 GHz, TDD
Subcarrier Spacing	30 kHz (0.5 ms slots)
Number of PRBs, band	273, 100 MHz
Max Transmit Power, \bar{P}	53 dBm, 0.73 W/PRB
gNB Antennas, spacing	12×8 cross-pol, 0.7λ rows, 0.5λ cols
UE Antennas, spacing	2 cross-pol elements 0.5λ
Spatial multiplexing	Up to rank 4 Single User MIMO
User Mobility	3 km/h

TABLE I. MAIN SIMULATION PARAMETERS

A single segment is configured to enforce a EIRP constraint over the whole sector $\gamma^* = \rho \bar{\gamma}$, where $\bar{\gamma}$ is the maximum EIRP that can be radiated by the gNB array by using the full 53 dBm transmit power and maximum array gain, and the power reduction factor is $\rho \in (0, 1]$. The outer-loop algorithm producing the per-period EIRP budget γ is implemented according to [9]. The PL techniques described in Section III are compared against the “Resource Limiting (RL)” baseline

used in [6], [7], where PRBs are consecutively allocated using $P_{u,k} = \bar{P}$ to UEs each slot as long as (9) is satisfied. The slot budget for “RL” and “PL” is computed via (5). The “PL - R” option implements the budget refinement as per (6), with $\rho^* = 0.1$ and $b^* = \gamma^*/10$. For reference, the curve without any EIRP control and power optimization [12] is plotted with the label “No EIRP Control”.

In Fig. 2 we compare the average cell throughput without actual EIRP control against different EMF-compliant techniques with $\rho = 1/4$ (or equivalently, -6 dB). The “No EIRP Control” curve shows how the carried load grows with increasing packet size, but saturating after a certain point, reaching 439 Mbits/s (black) at packet size $Q = 1.2$ Mbits. Once EIRP control has been activated, a lower carrier load is to be expected. The RL technique (blue) saturates much earlier with a carried load of 237 Mbits/s at $Q = 1.2$ Mbits, but still way above $1/4$ of “No EIRP Control” performance, thanks to the reduction in interference. Conversely, the PL techniques can be much closer to “No EIRP Control”, achieving up to 407 Mbits/s with the “PL - R” (red solid) and the hand-tuned $\epsilon = 0.9$. One can appreciate the slight yet consistent advantage of “PL - R” over the simple “PL” (green), along with the effects of different initial budget allocations in the period, represented by $\epsilon = 1.0, 0.5$ (red dashed, dotted), respectively.

In Fig. 3 we illustrate the average throughput perceived by each UE, defined as the ratio between the bits successfully received and the time taken for their reception. After an initial increase in UE throughput due to the higher carried traffic in the same time, reductions are observed with large packet size even in the absence of any actual EIRP limitation, due to the resource contention among UEs and the increased interference. In Fig. 3 we focus on just two EIRP control techniques, the best performing “PL - R” with $\epsilon = 0.9$ (red) versus the RL baseline [6], [7]. Then, we compare their performance with increasing EIRP limitations with $\rho = \{-3, -6, -9\}$ dB (cross, circle, plus markers), respectively. As expected, as ρ decreases, the UE throughput decreases with smaller packet sizes, corresponding to reduced offered load. However, we can notice the improvements brought by “PL - R”, that are more consistent when the power reduction factor ρ is smaller. This is due to the superposition of two effects discussed in [11], [12]. First of all, the throughput loss scales logarithmically with the transmitted power reduction. Moreover, the power optimization techniques [11], [12] applied by PL have the effect of stabilizing and reducing interference, resulting in a potentially higher peak performance. This trend is also evident in Fig. 3, where we observe gains of 5-8% at low loads compared to the ‘No EIRP Control’ case. When $\rho = -3$ dB, the UE throughput experiences a reduction of less than 1% at mid-high loads with “PL - R”.

All proposed EIRP control techniques discussed in this work successful enforced the desired EIRP limitation, although we do not provide explicit evidence due to space constraints.

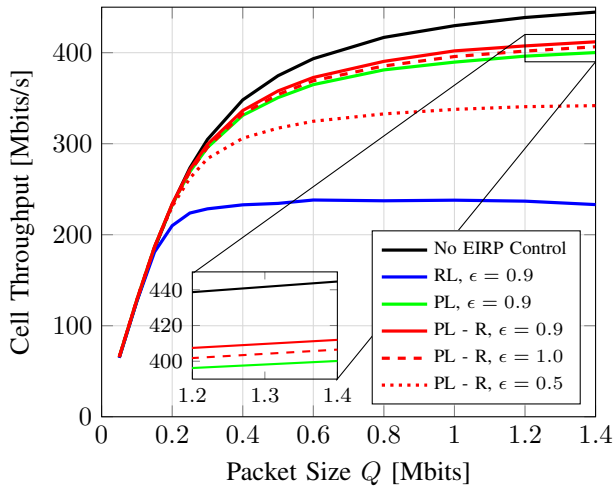


Fig. 2: Average cell throughput with different EIRP control techniques at constant $\rho = -6$ dB, benchmarked against the achievable performance without any EIRP control.

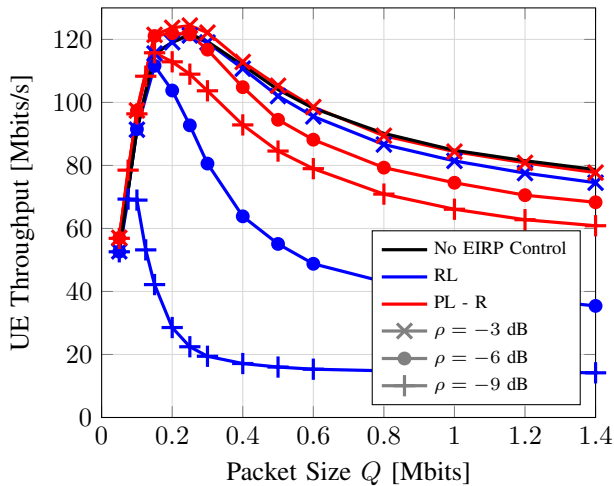


Fig. 3: Average UE throughput (defined as ratio between received bits and the time needed to receive them) without any power adaptation and EIRP control, for our best performing “PL - R” technique, and the baseline “RL”, as the power reduction factor ρ varies.

V. CONCLUSION

In this work we propose a set of techniques for EMF exposure mitigation that control the base station EIRP on a slot-per-slot basis to adhere to a budget defined over multiple slots. This budget is produced by an outer-loop algorithm such as the one in [9]. The integration of these two techniques enables a base station to comply with the “actual maximum approach” defined in [3]. Our solution reduces the transmission power fairly across all UEs with relatively low computational complexity. Moreover, it is fully parallelizable across different *segments*, that partition the sector into azimuth/elevation angle clusters on which configurable EIRP thresholds.

Our proposal significantly alleviates the impact of EMF mitigation constraints on user performance compared to legacy approaches that only adjust resource allocation without any power adaptation. For example, when the power reduction

factor is set to $1/4$ (or -6 dB), our method reduces cell throughput at high loads by a mere 6.5%, in contrast to a 44.2% reduction with the legacy approaches. The minimal computational overhead and the performance achieved in our detailed massive-MIMO simulation study confirm that our technique is a standout candidate for enforcing actual EIRP constraints in slot-by-slot operations of 5G and future 6G MAC schedulers.

ACKNOWLEDGEMENTS

The authors thank Tedros Abdu and Alois Herzog for the discussions and feedback during the evolution of this study.

REFERENCES

- [1] S. Wesemann, J. Du, and H. Viswanathan, “Energy efficient extreme MIMO: Design goals and directions,” *IEEE Communications Magazine*, 2023.
- [2] Int. Commission. on Non-Ionizing Radiation Protection (ICNIRP), “Guidelines for limiting exposure to electromagnetic fields (100 kHz to 300 GHz),” *Health physics*, vol. 118, no. 5, pp. 483–524, 2020.
- [3] Int. Electrotechnical Commission, “Determination of RF field strength, power density and SAR in the vicinity of radiocommunication base stations for the purpose of evaluating human exposure,” *IEC 62232:2022*.
- [4] P. Baracca, A. Weber, T. Wild, and C. Grangeat, “A statistical approach for RF exposure compliance boundary assessment in massive MIMO systems,” in *WSA 2018; 22nd International ITG Workshop on Smart Antennas*. VDE, 2018, pp. 1–6.
- [5] M. Rybakowski, K. Bechta, C. Grangeat, and P. Kabacik, “Impact of Beamforming Algorithms on the Actual RF EMF Exposure From Massive MIMO Base Stations,” *IEEE Access*, 2023.
- [6] C. Törnevik, T. Wigren, S. Guo, and K. Huisman, “Time averaged power control of a 4G or a 5G radio base station for RF EMF compliance,” *IEEE Access*, vol. 8, pp. 211 937–211 950, 2020.
- [7] T. Wigren and C. Törnevik, “Coordinated average EIRP control of radio transmitters for EMF exclusion zone computation,” *IEEE Wireless Communications Letters*, vol. 10, no. 9, pp. 2075–2079, 2021.
- [8] M. R. Castellanos, D. J. Love, and B. M. Hochwald, “Hybrid precoding for millimeter wave systems with a constraint on user electromagnetic radiation exposure,” in *2016 50th Asilomar Conference on Signals, Systems and Computers*. IEEE, 2016, pp. 296–300.
- [9] L. Maggi, A. Herzog, A. Zejnilagic, and C. Grangeat, “Smooth Actual EIRP Control for EMF Compliance with Minimum Traffic Guarantees,” *arXiv:2404.06624*, 2024.
- [10] P. Kela, J. Puttonen, N. Kolehmainen, T. Ristaniemi, T. Henttonen, and M. Moision, “Dynamic packet scheduling performance in UTRA long term evolution downlink,” in *2008 3rd International Symposium on Wireless Pervasive Computing*. IEEE, 2008, pp. 308–313.
- [11] S. Mandelli, A. Lieto, P. Baracca, A. Weber, and T. Wild, “Power optimization for low interference and throughput enhancement for 5G and 6G systems,” in *2021 IEEE Wireless Communications and Networking Conference Workshops (WCNCW)*. IEEE, 2021, pp. 1–7.
- [12] S. Mandelli, A. Lieto, M. Razenberg, A. Weber, and T. Wild, “Reducing interference via link adaptation in delay-critical wireless networks,” *EURASIP Journal on Wireless Communications and Networking*, vol. 2022, no. 1, p. 109, 2022.
- [13] J. Mo and J. Walrand, “Fair end-to-end window-based congestion control,” *IEEE/ACM Transactions on networking*, vol. 8, no. 5, pp. 556–567, 2000.
- [14] S. P. Boyd and L. Vandenberghe, *Convex optimization*. Cambridge university press, 2004.
- [15] 3GPP, “TR 38.901. Study on channel model for frequencies from 0.5 to 100 GHz,” Technical Report, 2023.
- [16] M. D. Zoltowski, M. Haardt, and C. P. Mathews, “Closed-form 2-D angle estimation with rectangular arrays in element space or beamspace via unitary ESPRIT,” *IEEE Transactions on Signal Processing*, vol. 44, no. 2, pp. 316–328, Feb. 1996.
- [17] 3GPP, “TR 36.814. Further advancements for E-UTRA physical layer aspects,” Technical Report, 2017.
- [18] —, “TS38.214. NR; Physical layer procedures for data,” Technical Specification, 2020.